

This discussion paper is/has been under review for the journal Atmospheric Chemistry and Physics (ACP). Please refer to the corresponding final paper in ACP if available.

Aerosol concentration and size distribution measured below, in, and above cloud from the DOE G-1 during VOCALS-REx

L. I. Kleinman¹, P. H. Daum¹, Y.-N. Lee¹, E. R. Lewis¹, A. J. Sedlacek III¹,
G. I. Senum¹, S. R. Springston¹, J. Wang¹, J. Hubbe², J. Jayne³, Q. Min⁴,
S. S. Yum⁵, and G. Allen⁶

¹Brookhaven National Laboratory, Upton, New York, USA

²Pacific Northwest National Laboratory, Richland, Washington, USA

³Aerodyne Research Inc., Billerica, Massachusetts, USA

⁴State University of New York, Albany, New York, USA

⁵Yonsei University, Seoul, 120749, South Korea

⁶University of Manchester, Manchester, M13 9PL, UK

Received: 19 May 2011 – Accepted: 23 May 2011 – Published: 21 June 2011

Correspondence to: L. I. Kleinman (kleinman@bnl.gov)

Published by Copernicus Publications on behalf of the European Geosciences Union.

17289

Abstract

During the VOCALS Regional Experiment, the DOE G-1 aircraft was used to sample a varying aerosol environment pertinent to properties of stratocumulus clouds over a longitude band extending 800 km west from the Chilean coast at Arica. Trace gas and aerosol measurements are presented as a function of longitude, altitude, and dew point in this study. Spatial distributions are consistent with an upper atmospheric source for O₃ and South American coastal sources for marine boundary layer (MBL) CO and aerosol, most of which is acidic sulfate in agreement with the dominant pollution source being SO₂ from Cu smelters and power plants. Pollutant layers in the free troposphere (FT) can be a result of emissions to the north in Peru or long range transport from the west. At a given altitude in the FT (up to 3 km), dew point varies by 40 °C with dry air descending from the upper atmospheric and moist air having a BL contribution. Ascent of BL air to a cold high altitude results in the condensation and precipitation removal of all but a few percent of BL water along with aerosol that served as CCN. Thus, aerosol volume decreases with dew point in the FT. Aerosol size spectra have a bimodal structure in the MBL and an intermediate diameter unimodal distribution in the FT. Comparing cloud droplet number concentration (CDNC) and pre-cloud aerosol ($D_p > 100$ nm) gives a linear relation up to a number concentration of ~ 150 cm⁻³, followed by a less than proportional increase in CDNC at higher aerosol number concentration. A number balance between below cloud aerosol and cloud droplets indicates that ~ 25 % of aerosol in the PCASP size range are interstitial (not activated). One hundred and two constant altitude cloud transects were identified and used to determine properties of interstitial aerosol. One transect is examined in detail as a case study. Approximately 25 to 50 % of aerosol with $D_p > 110$ nm were not activated, the difference between the two approaches possibly representing shattered cloud droplets or unknown artifact. CDNC and interstitial aerosol were anti-correlated in all cloud transects, consistent with the occurrence of dry in-cloud areas due to entrainment or circulation mixing.

components of sub micrometer size aerosol measured by the AMS (RI=1.46). Addition of retained water (RI=1.33) results in a lower refractive index, close to 1.41.

Comparisons were made between aerosol volume determined by the SMPS and the two PCASPs. In order to match size ranges, volumes are calculated for D_p between 0.11 and 0.44 μm . A linear regression of PCASP A volume vs. SMPS volume had a slope of 0.84 and $r^2 = 0.91$; for PCASP B the slope and r^2 were 0.98 and 0.93, respectively. Agreement is well within the 30% uncertainty limits typically cited for PCASP and SMPS volume measurements. Volumes determined by PCASP A and B vary by only a few percent according to which unit is inside or outside of the aircraft.

PCASP and SMPS number distributions differed, primarily due to a low detection efficiency of small particles in the PCASP ($D_p < 160 \text{ nm}$), which was confirmed only recently in a post-flight calibration of PCASP A. PCASP size distributions were adjusted to match those from the SMPS. A set of global adjustment factors to be applied to all PCASP data were determined by performing a linear regression between the SMPS and PCASP A and PCASP B for 15 size bins. All non-cloud data were used for these regressions. To test the normalization procedure, plots were made of PCASP vs. SMPS number concentration integrated over the overlap size range 110–440 nm (not shown). A least squares regression yields slopes of 0.95 and 0.96 for PCASP A and B vs. SMPS, respectively, both with an r^2 of 0.85. By construction slopes should be close to unity. Scatter in the number comparisons is a measure of how well a single set of adjustment factors works in the differing environments encountered over 16 flights. Normalization resulted in an increase of total particle concentration by 41% and 18% from PCASP A and PCASP B, respectively.

By adjusting the PCASP data, we are relying on the SMPS as providing an intrinsically more accurate size distribution. The adjustment procedure allows for the determination of number concentrations and size distributions with 1 s time resolution using PCASP data which on average agrees with the SMPS. Fast response aerosol number concentrations will prove useful in examining the anti-correlation between cloud droplets and interstitial aerosol.

17295

2.1.3 Cloud microphysics

Cloud droplet number concentration (CDNC) was determined via a Cloud and Aerosol Spectrometer (CAS) probe manufactured by Droplet Measurement Technologies (DMT). Results were integrated over a diameter range between 2.5 and 50 μm . Cloud liquid water content (LWC) was measured with a Particle Volume Monitor (PVM, Gerber et al., 1994) and checked against a hot wire detector. Drizzle concentration was determined from a DMT Cloud Imaging Probe (CIP) which together with the CAS and hot wire detector are packaged together as a Cloud, Aerosol, and Precipitation Spectrometer (CAPS), mounted on a pylon off the nose of the G-1. Data has been archived at 0.1, 1, and 10 Hz, and is available on request at 40 and in some cases 200 Hz.

2.2 Flights

Figure 1 shows the 3-D sampling region of the G-1 during 16 of 17 research flights. An electrical failure on 18 October limited data collection and that flight is not used in this study. Instrument status and flight times are tabulated in spreadsheet format on the same ftp site as the data. Flight duration was approximately 4 h. Thirteen of 16 flights started between 08:57 and 10:20 (11:57 and 13:20 UTC).

Flight objectives were to determine the horizontal and vertical variability of cloud and aerosol properties. The range of the G-1 allowed for sampling between Arica at 70.3° W out over the Pacific to 78° W, an E–W distance of 800 km. Vertical sampling was done either via multiple transects at different altitudes, ascents and descents through clouds typically at vertical velocities of 1000 ft min^{-1} , or by porpoising between cloud and above-cloud regions.

A typical flight track designed to sample longitudinal variations in cloud and aerosol properties is shown in Fig. 2. Because clouds thinned and sometimes disappeared due to solar heating as the day progressed, the out bound leg was usually devoted to cloud sampling and the inbound leg to sampling in the boundary layer below cloud height. In order to examine interstitial aerosol, 102 constant altitude transects were identified

17296

in which the maximum liquid water content (LWC) was at least 0.1 g m^{-3} . Often there were multiple transects in a single cloud separated by a step change in altitude of order tens of m or greater. For many transects clouds were broken or occupied only a portion of the transect. The non-cloud ($\text{LWC} < 0.01 \text{ g m}^{-3}$) portion of these transects defines precloud aerosol that can be compared with interstitial size distributions as a function of LWC. One cloud on Flight 081028a (Fig. 2) is singled out as a case study to illustrate the anti-correlation between cloud droplet number concentration and interstitial aerosol found in all 102 cloud transects. As described in Sect. 3.3, an alternate definition of pre-cloud aerosol related to aerosol below cloud height is used to quantify the first indirect effect.

As indicated in Fig. 3, aerosol number concentration measured by SMPS was nearly the same on outbound and inbound legs, even though below-cloud measurements at a particular longitude could be separated by 500 m in altitude and more than 3 h in time. On average, pre-cloud aerosol can be represented by low altitude samples collected at the same longitude.

There were 3 intercomparison flights between the G-1 and C130, BAe-146 and Twin Otter that yielded data on LWC and CDNC (from a CDP or CAS probe). Results are summarized in Table 2. Intercomparisons were conducted with a several minute time separation between aircraft. Small differences in location, especially altitude, had a large influence on LWC. More significant are differences in CDNC where the G-1 values have to be reduced by 10, 17 and 38 % to match the C130, TO, and BAe146, respectively. Although the comparison with the BAe146 is based on a short sample through broken clouds, a particle balance between below cloud and in-cloud is consistent with the G-1 CDNC being approximately 20 % too high – of the same order as published estimates of measurement uncertainty (Fountoukis et al., 2007). This factor also agrees with inter-platform differences in CDNC vs. longitude (not shown).

17297

3 Results

Source regions for aerosol and trace gases have been analyzed by Allen et al. (2011) and Bretherton et al. (2010) by means of back trajectories calculated for the marine boundary layer (MBL) at 950 hPa and free troposphere (FT) at 850 hPa starting from 20° S at distances from the shore varying from 70.5° W to 90° W . Much of this work is pertinent to the longitudinal and vertical pollutant distribution measured by the G-1. Allen et al. (2011) and Bretherton et al. (2010) found that pollutants in the near coastal MBL could be explained by low altitude winds from the S and SE that intersected the Chilean coast. Trajectories terminating further offshore where pollution levels are lower tend to remain off shore, missing coastal emission sources. FT back trajectories were more diverse. In one population, descending air from the direction of Australia and South Asia carried pollutants to the VOCALS region. Another category of FT trajectory prevalent between the coast and 75° W were northerlies from Peruvian coastal regions. A contribution to the FT consisting of return coastal flow from the MBL is hypothesized by Allen et al. (2011) based on instances with high humidity and low O_3 .

3.1 Spatial distributions

Data have been segregated into marine boundary layer, pre-cloud, in-cloud, and free tropospheric subsets as defined in Table 3. Pre-cloud aerosol is an approximation to the aerosol actually ingested into a cloud, justified by observations such as presented in Fig. 3. Clouds were located primarily between 800 and 1200 m altitude with cloud base and inversion height increasing with distance from the shore (Rahn and Garreaud, 2010; Bretherton et al., 2010).

Figure 4 shows frequency distributions of sub-micrometer aerosol number and volume concentration and CO and O_3 mixing ratio as a function of longitude for the below cloud layer. Aerosol number concentration and volume decrease 2.3 and 3.6-fold, respectively between 70° and 75° W , the difference between number and volume appearing in the aerosol size distributions, presented below. There is a monotonic decrease in

17298

expected, concentrations in the limited geographic area covered by the G-1 increase with distance from the coast. The VOCALS region, unlike the remote Pacific, is characterized by strong subsidence and it is likely that the source of O_3 in the MBL towards the west is subsidence from the FT. Indeed, O_3 from the FT is used as an inert tracer to quantify cloud top entrainment (e.g., Faloon et al., 2005). Aerosol particles will be entrained as a component of FT O_3 containing air. Although large particles in the FT are fewer than in the MBL (Sect. 3.2, following), they can, as shown by Clarke et al. (1996, 1997), provide CCN to replace those lost by drizzle – a process of particular importance in the drizzled out POC regions further west than the G-1 sampled (Wood et al., 2011).

In the MBL, CO is anti-correlated with O_3 consistent with the oppositely directed east-west trends shown in Fig. 4c,d. Emission sources are located on land which lends some logic to CO concentrations being highest near the shore but does not address the near-shore O_3 which not only is low but is also anticorrelated with CO. CO– O_3 anticorrelations of the type observed in winter by Parrish et al. (1998) do not seem relevant in the low NO_x VOCALS region. Allen et al. (2011) suggest the possible effects of fresh emissions but also note that a transport process may be responsible. An explanation for the low near-shore O_3 may have to await process analysis of CTM results.

The anti-correlation between CO and O_3 disappears at the 0 to -20°C dew point level and in the driest air is replaced with a significant positive correlation due to long range transport of pollution plumes. An extreme example occurred on Flight 081025a and is identified on Fig. 7. The polluted layer was at 74.5°W between 2300 and 2500 m altitude. Dew point at -40°C was among the driest observed. Insoluble pollutants, CO and O_3 averaged 115 and 83 ppb, the highest levels observed during the campaign. Aerosol number and volume were several-fold less than at lower altitude but were the highest values observed in such dry air. Ten day back trajectories generated from the HYSPLIT model (Draxler and Rolph, 2010) descend from high altitude ($> 7000\text{ m}$) over the Pacific but are inconclusive regarding the origin of this air mass. As CO definitely

17301

has a boundary layer source, these descending air parcels maintain a chemical record of a prior boundary layer residence.

In order not to distort statistical relations by a single high concentration plume, correlations for data with dew point between -20 and -40°C have been calculated with and without data from 25 October. With the 25 October plume, a reduced major axis least squares regression yields a CO to O_3 ratio of 1.0 with an r^2 of 0.68. Removing the 25 October data yields a CO to O_3 ratio of 1.2 with an r^2 of 0.41. Both values indicate very efficient O_3 production and/or loss of O_3 in transport as compared with surface observations that have a CO/ O_3 ratio a factor of 3 lower (Parrish et al., 1998). The 25 October plume shows up in the concentrations of aerosol sulfate and even more in organic aerosol (Fig. 7). A linear regression between organic aerosol and CO gives a ratio of $7.2\ \mu\text{g m}^{-3}\ \text{ppm}^{-1}$ CO ($r^2 = 0.56$). A similar ratio of $6.9\ \mu\text{g m}^{-3}\ \text{ppm}^{-1}$ CO is obtained without data from 25 October. These values are an order of magnitude lower than found in polluted boundary layer air masses after about one day of photochemical processing (Kleinman et al., 2008), indicating precipitation removal of aerosol.

In addition to the CO plumes observed in the driest air there are observations of high CO ($> 80\text{ ppb}$) concentration, located over a range of altitudes with dew points between 0 and 6°C (i.e. in the bin just above the cloud layer). CO in these cases is anti-correlated with O_3 . HYSPLIT back trajectories intercept or come close to the Peruvian coast in agreement with wind measurements presented by Bretherton et al. (2010) and Rahn and Garreaud (2010). Bretherton et al. (2010) note that heating of the Andean slope mixes moisture into a layer that becomes the lower free troposphere when advected over the Pacific. High concentrations of CO in the moist above cloud layer are further evidence of the upward mixing of continental boundary layer air. The next driest bin in Fig. 6 also has data points with high CO. Here the anti-correlation between CO and O_3 has changed into a lack of correlation.

Concentrations of aerosol sulfate and organics both decrease with altitude (Lee et al., 2011) or dew point (Fig. 7). There is a selective reduction in aerosol sulfate in dry air which could reflect a greater solubility and propensity for wet removal, relative

17302

in-cloud aerosol measurements, but results will be biased high from shattered cloud droplets counted as aerosol particles. Despite this shortcoming, interstitial aerosol will be discussed using the later approach because co-located cloud and aerosol measurements allows a connection to be made with cloud microphysics. In-situ data for N_{int} includes broken clouds which leads to a further increase relative to data in Fig. 10.

Most clouds contained significant numbers of interstitial aerosol particles. This can be seen from the number balance in Fig. 10 for $N_{\text{int}} > 200 \text{ cm}^{-3}$ and from in-cloud observations in Fig. 11 in which average size spectra from the inside-cabin PCASP are given as a function of cloud liquid water content. Comparison is made to an average size distribution determined in cloud free air located along the same 102 constant altitude transects used for the cloud data. Although individual transects may not have cloud free portions, on average cloud free aerosol is nearly identical to pre-cloud aerosol defined in Table 3. Aerosol and LWC data are presented in Fig. 11 at 1 s time resolution, equivalent to an average over 100 m distance. Data from the in-cabin PCASP is available at 10 Hz but the added time resolution is defeated by uncertainties in sampling time and poor counting statistics. As shown below and as demonstrated in other measurement campaigns (e.g., Gerber et al., 2005) there is significant cloud structure including holes at smaller spatial scales. For the purpose of interpreting Fig. 11, sub 1 s structure effects results to the extent that the PCASP spectra are assigned to an incorrect LWC category. In particular, aerosol in short duration holes appear as a contribution to N_{int} at a LWC determined by a 1 s average.

Figure 11 shows a monotonic decrease in interstitial aerosol as cloud liquid water is increased. For clouds with $\text{LWC} > 0.1 \text{ g m}^{-3}$, the fraction of aerosol not activated changes from 47 % to 26 % as LWC is increased to above 0.6 g m^{-3} . The fraction of aerosol that is interstitial decreases markedly at large diameter, as has been found in multiple studies (e.g., Gillani et al., 1995).

Cloud droplet shatter contributes to N_{int} . In-cloud SMPS size spectra show extremely high concentrations of small particles, i.e. 10^3 to more than 10^4 particles cm^{-3} smaller than 50 nm diameter. Similar concentrations of small particles in-cloud have been

17305

previously observed and attributed to droplet shatter (e.g., Hudson and Frisbie, 1991; Clarke et al., 1997; Weber et al., 1998). Given extremely high concentrations of small particles due to droplet shatter, the much less numerous accumulation mode aerosol do not stand out. Rather, they appear as a shoulder or sometimes a bump in the size distribution that is quantifiable as a separate mode by fitting the distribution to a sum of log normals, as illustrated in Fig. 12. In this case, a small percentage of in-cloud particles large enough to be detected by the PCASP are part of a tail on the shatter distribution and the majority appear to be part of a mode that is distinct from the shatter size distribution. According to the fitted log normals for 102 cloud transects, the shatter mode within the PCASP size range can vary between zero and several 10's of percent of the accumulation mode, with very few occurrences of particles as large as 200 nm. Although, the log normal fits are suggestive, there is no a priori reason why cloud droplet shatter should have this functional form, which leaves in doubt the quantitative apportionment of larger particles between droplet shatter and interstitial aerosol.

Both in and out of cloud, the number of particles larger than 600 nm is small. There is no evidence that the inside PCASP (or SMPS) is detecting partially evaporated cloud droplets in contrast to what has been observed for particles with $D_p > 400\text{--}500 \text{ nm}$, measured outside of the cabin (Leaich et al., 1996). The absence of these particles inside the cabin is a consequence of cloud droplets being too large to go through the aerosol inlet. Extra drying, beyond that supplied by a deicing heater, due to adiabatic compression and cabin heat also contributes. Size distribution measurements from the nose mounted PCASP, in contrast show a population of in-cloud particles with $D_p > 500 \text{ nm}$ that can be more numerous than the sub 500 nm population.

Interstitial aerosol representing evaporated cloud droplets or aerosol particles that did not activate were anti-correlated with CDNC in all clouds sampled by the G-1. Similar observations have been made by others (e.g., Gultepe et al., 1996). As a representative example we consider a case study cloud observed on Flight 081028a, centered at 75.2° W (Fig. 2). Figure 13a shows a 1 Hz time series of CDNC and N_{int} measured

17306

with the CAS and inside-cabin PCASP, respectively. There are multiple spikes lasting no more than 1 s in which a decrease in CDNC is accompanied by an increase in N_{int} . There are also variations on time scales of tens of seconds or longer in which the relation between CDNC and N_{int} is less apparent.

5 A plot of CDNC vs. N_{int} (Fig. 13b) shows an overall anti-correlation but with considerable scatter. The anti-correlation that is apparent in the high frequency spikes in Fig. 13a is partially obscured by changes in pre-cloud aerosol and/or cloud dynamics that are important over spatial scales of order 5 km and greater. In order to account for the non-uniformity of the cloud, we qualitatively separate low and high frequency components. A 400 s binomial filter, subjectively selected, has been applied, yielding low
10 frequency components shown by red lines in Fig. 13a. High frequency components called anomalies to avoid confusion with 10 Hz data presented later on are defined as the difference between a 1 Hz signal and the corresponding low frequency filtered component. A graph of high frequency anomalies in Fig. 13c has reduced scatter.

15 Low frequency changes in aerosol and cloud droplets contribute to scatter in Fig. 13b. Cloud regions which have different aerosol inputs or different dynamics can have CDNC vs. aerosol plots that are shifted relative to each other. In Fig. 13d, the original 1 s data has been subject to a 10 s running box car average, which is a visual aid to picking out contiguous points. Lines are drawn between consecutive data
20 points and color coded to correspond to the time sequence in Fig. 13a. One can pick out 4 or 5 strands that represent contiguous cloud portions up to 10 km in length that individually show an anti-correlation between CDNC and N_{int} . Among the 102 clouds transects, this type of structure is common. At a still larger spatial scale approaching the length of the transect, CDNC and N_{int} are correlated (Fig. 13e). Depending on
25 mesoscale structure, the low frequency changes in CDNC and N_{int} can be correlated, anti-correlated, or scattered.

Higher frequency measurements are useful in interpreting the presence of interstitial aerosol. Increasing the time response of cloud droplet measurements to 10 Hz as in Fig. 14, shows that the cloud contains regions in which CDNC decreases to near zero

17307

accompanied by large decreases in LWC but relatively small changes in volume mean radius. It is expected that the interstitial aerosol shows similar high frequency structure but this is not observable with our sampling line.

5 A regression between the high frequency components of CDNC and accumulation mode aerosols has a slope of -2.0 for the case study cloud in Figs. 13 and 14, approximately equal to the median slope of -2.1 found for the entire data set of 102 clouds. Several factors contribute to the slope being steeper than minus 1, the value that would be obtained if removal of a single cloud droplet resulted in the appearance
10 of an interstitial aerosol particle detected by the PCASP. First is the possibility of an overestimate in CDNC as suspected from the intercomparison data in Table 2. If actual CDNC are 80 % of measured, correcting the CDNC changes the slope by a factor of 0.8 (i.e. from -2 to -1.6). Second, cloud droplets could be formed from aerosol particles smaller than the 110 nm lower limit of detection of the PCASP. Sub-cloud aerosol size distributions have a Hoppel minimum at ~ 75 nm, indicating that sometime in the
15 air mass history, particles of that size were CCN (Cantrell et al., 1999). Third, and likely most important, is a degraded time response due to mixing in the inlet manifold leading to the inside-cabin PCASP. This effect has been simulated by constructing a PCASP signal which is the negative of CDNC, then subjecting it to 3 point binomial smoothing to simulate mixing. The resulting regression slope between the high frequency components
20 of CDNC and the synthetic PCASP signal was -1.49 , instead of -1 before smoothing. Results depend on the degree of smoothing and our choice is meant to be only illustrative. Supporting evidence for the importance of time response comes from the PCASP mounted on the aircraft nose which yields a median slope of -1.35 .

17308

large particles to remain unactivated. However as pointed out by Guibert et al. (2003) particles respond to the supersaturation existing along their trajectories and a very low vertical velocity at cloud base may not be persistent.

High concentrations of interstitial particles can be caused by low hygroscopicity. Organic coating and kinetic limitations have been discussed in the literature as ways of slowing down the activation process (Chuang et al., 1997; Nenes et al., 2001; Feingold and Chuang, 2002). Although these effects cannot be discounted we view them as unlikely due to the predominance of a single hygroscopic aerosol type, the domain over which kinetic effects are significant, and the low fraction of organic material.

Cloud top entrainment of dry air evaporates cloud droplets returning aerosol particles to the interstitial phase. Depending on the horizontal dimensions of the entrained air the time sequence of anti-correlated CDNC and N_{int} (Fig. 13a) will be more or less spiky as observed from a moving platform. We have shown 1 Hz and 10 Hz data but it is known that clouds are inhomogeneous on smaller scales. Cloud top entrainment of dry air in Sc sampled during DYCOMS II was observed to produce holes with an average width (short dimension) of 5 m. These holes are defined by having reduced LWC compared with non-hole background areas (Gerber et al., 2005). The occurrence of dry areas within a 1 s, 100 m sampling interval is a possible mechanism for generating an aerosol particle that is called interstitial because on a 100 m spatial scale it is in a cloud but actually resides in clear air. Another way of generating dry holes is through a circulation mechanism that causes variations in local cloud base height such that at low altitude where LWC is low there are more encounters with clear air and therefore a higher N_{int} . In agreement with the circulation mechanism, Wang et al. (2009) find altitude gradients in LWC, CDNC, and N_{int} in Sc during the MASE campaign that produce a result observed here, namely that interstitial aerosol decreases at high LWC (their Fig. 2d–f).

17311

5 Conclusions

During the VOCALS-REx field campaign, the DOE G-1 covered a longitude range between Arica on the coast of Chile (70.3° W) and 78° W, an 800 km distance over which MODIS retrievals show a strong gradient in CDNC and effective radius. Aerosol number and volume concentration in the MBL decreased with off-shore distance with most of the decrease occurring between the coast and 75° W. This pattern is consistent with the trajectory analysis of Allen et al. (2011) and Bretherton et al. (2010) that indicate a source region to the south along the Chilean coast, whose impact is felt most often east of 75° W and with decreasing frequency further west. MBL concentrations of O_3 increase with distance from the coast while CO concentrations decrease indicating a nearby continental source for the latter.

Aerosol in the MBL is acidic sulfate with a 10–15 % admixture of organics consistent with emissions dominated by Cu smelters and power plants (Lee et al., 2011). MBL aerosol have an Aitken and accumulation mode with geometric mean diameters of 45–60 nm and 160–185 nm, respectively, separated by a Hoppel minimum. In the FT, number size distributions are unimodal and broad, centered at 90 nm.

In each of three altitude ranges, collectively spanning the FT from 1200 to 3000 m, dew point varied by more than 40 °C, showing that within a narrow altitude span, air masses with very different histories were sampled. The requirement that an ascending air mass has a relative humidity less than 100 %, combined with a strong dependence of temperature on altitude implies that the lowest dew point air observed (–40 °C) originated above 8 km altitude (assuming a surface temperature of 15 °C and a lapse rate of 6.5 °C km^{–1}). Conversely, moist air implies a low altitude source.

Frequency distributions of CO, O_3 , aerosol number, and aerosol volume are provided as functions of altitude and dew point. Using dew point in place of altitude has the advantage of separating air masses according to history and highlights the different behavior of soluble and insoluble pollutants (Kleinman and Daum, 1991). Dew point more clearly picks up trends in O_3 because O_3 has a source in the dry upper atmosphere

17312

and a MBL sink. There is a pronounced decrease in aerosol volume with dew point as low dew point air masses have been subject to cloud processes that have removed all but a few percent of their total water. Removed along with water are soluble substances such as accumulation mode particles that are CCN. The decrease with dew point of aerosol number concentration is less extreme because of the dominance of smaller less easily activated particles in the FT. The FT population of aerosol, however, does contain some accumulation mode size particles ($D_p > 100$ nm) which will subside into the MBL, much the same as O_3 , thereby providing a source of CCN to replace that lost by drizzle (Clarke et al., 1996, 1997). Relative solubility may play a role in the 5 fold increase in the organic aerosol to sulfate ratio with decreasing dew point. It is also possible that the high ratio at low T_d reflects emission rates in areas not dominated by Cu smelters and power plants. Even with an elevated organic to sulfate ratio in dry air, the organic aerosol to CO ratio is an order of magnitude lower than observed in day old plumes in the boundary layer in other field studies.

One hundred and two constant altitude cloud transects were identified and used to examine relations between CDNC and the number concentration of interstitial aerosol (N_{int}) as measured by a heated PCASP inside the aircraft cabin. In each transect CDNC and N_{int} are anti-correlated, suggesting that a decrease in cloud droplets by e.g. mixing or evaporation leads to the appearance of interstitial aerosol. One cloud sampled over a 35 km transect was selected for a case study. Within this cloud there were 4 or 5 regions with distinctly different relations between CDNC and N_{int} contributing to scatter over the 35 km cloud. Much of the scatter could be removed by applying a high pass filter and examining the anomalies determined as the total signal less the low frequency variation.

Measurements from the inside-cabin PCASP indicate that between 1/4 ($LWC > 0.6 \text{ g m}^{-3}$) and 1/2 ($LWC = 0.1$ to 0.2 g m^{-3}) of aerosol particles with $D_p > 110$ nm remain as interstitial during cloud transects. A comparison of pre-cloud air with CDNC yields an interstitial fraction of 1/4. Adiabatic parcel model calculations based on measured aerosol composition, concentration, size distribution, and a 0.4 cm s^{-1} vertical

17313

velocity show that most aerosol in the PCASP size range should be activated. It is possible that a portion of the interstitial aerosol is derived from shattered cloud droplets or from an unknown artifact. Leaving aside measurement uncertainties there are several possible explanations, namely that some air parcels had less than average vertical velocities, particles were never activated, or that cloud droplets evaporated. Creation of dry holes by cloud top entrainment or a circulation mechanism that causes variations in local cloud base height need to be considered.

Acknowledgement. We thank chief pilot Bob Hannigan and the flight crew from PNNL for a job well done. We gratefully acknowledge the Atmospheric Science Program within the Office of Biological and Environmental Research of DOE for supporting field and analysis activities and for providing the G-1 aircraft. Use of a c-ToF-AMS provided by EMSL is appreciated. The VOCALS Regional Experiment owes its success to many people. We would like to single out Robert Woods (Univ. of Washington), Christopher Bretherton (Univ. of Washington), and C. Roberto Mechoso (UCLA) for their organizational skills and scientific leadership. S. S. Yum is partially supported by the Korean Meteorological Administration Research and Development Program under Grant RACS 2010-5001. This research was performed under sponsorship of the US DOE under contracts DE-AC02-98CH10886.

References

- Allen, G., Coe, H., Clarke, A., Bretherton, C., Wood, R., Abel, S. J., Barrett, P., Brown, P., George, R., Freitag, S., McNaughton, C., Howell, S., Shank, L., Kapustin, V., Brekhovskikh, V., Kleinman, L., Lee, Y.-N., Springston, S., Toniazzo, T., Krejci, R., Fochesatto, J., Shaw, G., Krecl, P., Brooks, B., McMeeking, G., Bower, K. N., Williams, P. I., Crosier, J., Crawford, I., Connolly, P., Allan, J. D., Covert, D., Bandy, A. R., Russell, L. M., Trembath, J., Bart, M., McQuaid, J. B., Wang, J., and Chand, D.: South East Pacific atmospheric composition and variability sampled along 20° S during VOCALS-REx, *Atmos. Chem. Phys.*, 11, 5237–5262, doi:10.5194/acp-11-5237-2011, 2011.
- Ayers, G. P., Penkett, S. A., Gillett, R. W., Bandy, B., Galbally, I. E., Meyer, C. P., Elsworth, C. M., Bentley, S. T., and Forgan, B. W.: Evidence for photochemical control of ozone concentrations in unpolluted marine air, *Nature*, 360, 446–449, 1992.

17314

- Hubbe, J., Zaveri, R. A., Brechtel, F. J., Jayne, J., Onasch, T. B., and Worsnop, D.: Aircraft observations of aerosol composition and ageing in New England and Mid-Atlantic States during the summer 2002 New England Air Quality Study field campaign, *J. Geophys. Res.*, 112, D09310, doi:10.1029/2006JD007786, 2007.
- 5 Kleinman, L. I., Springston, S. R., Daum, P. H., Lee, Y.-N., Nunnermacker, L. J., Senum, G. I., Wang, J., Weinstein-Lloyd, J., Alexander, M. L., Hubbe, J., Ortega, J., Canagaratna, M. R., and Jayne, J.: The time evolution of aerosol composition over the Mexico City plateau, *Atmos. Chem. Phys.*, 8, 1559–1575, doi:10.5194/acp-8-1559-2008, 2008.
- 10 Kley, D., Crutzen, P. J., Smit, H. G. J., Vömel, H., Oltmans, S. J., Grassl, H., and Ramanathan, V.: Observations of near-zero ozone concentrations over the convective Pacific: effects on air chemistry, *Science*, 274, 230–233, 2006.
- Leaitch, W. R., Banic, C. M., Isaac, G. A., Couture, M. D., Liu, P. S. K., Gultepe, I., Li, S.-M., Kleinman, L. I., Daum, P. H., and MacPherson, J. I.: Physical and chemical observations in marine stratus during the 1993 North Atlantic Regional Experiment: factors controlling cloud droplet number concentrations, *J. Geophys. Res.*, 101, 29123–29135, 1996.
- 15 Lee, Y.-N., Springston, S., Jayne, J., Wang, J., Senum, G., Hubbe, J., Alexander, L., Brioude, J., Spak, S., Mena-Carrasco, M., Kleinman, L., and Daum, P.: Aerosol composition, chemistry, and source characterization during the 2008 VOCALS Experiment, *Atmos. Chem. Phys. Discuss.*, in preparation, 2011.
- 20 Liu, Y. and Daum, P. H.: The effect of refractive index on size distributions and light scattering coefficients derived from optical particle counters, *J. Aerosol Sci.*, 8, 945–957, 2000.
- Nenes, A., Ghan, S., Abdul-Razzak, H., Chuang, P. Y., and Seinfeld, J. H.: Kinetic limitations on cloud droplet formation and impact on cloud albedo, *Tellus B*, 53, 133–149, 2001.
- Parrish, D. D., Trainer, M., Holloway, J. S., Yee, J. E., Warshawsky, M. S., Fehsenfeld, F. C., Forbes, G. L., and Mody, J. L.: Relationship between ozone and carbon monoxide at surface sites in the North Atlantic region, *J. Geophys. Res.*, 103, 13357–13376, 1998.
- 25 Rahn, D. A. and Garreaud, R.: Marine boundary layer over the subtropical southeast Pacific during VOCALS-REx – Part 1: Mean structure and diurnal cycle, *Atmos. Chem. Phys.*, 10, 4491–4506, doi:10.5194/acp-10-4491-2010, 2010.
- 30 Ramanathan, V., Crutzen, P. J., Kiehl, J. T., and Rosenfeld, D.: Aerosols, climate, and the hydrological cycle, *Science*, 294, 2119–2124, 2001.
- Robinson, N. F.: The efficient numerical calculation of condensational cloud droplet growth, *J. Atmos. Sci.*, 41, 698–700, 1984.

17317

- Schwartz, S. E. and Slingo, A.: Enhanced shortwave cloud radiative forcing due to anthropogenic aerosols, in: *Clouds, Chemistry and Climate, Proceedings of NATO Advanced Research Workshop, Ringberg, Germany, 21–25 March 1994*, edited by: Crutzen, P. and Ramanathan, V., Springer, Heidelberg, 191–236, 1996.
- 5 Snider, J. R. and Brenguier, J.-L.: Cloud condensation nuclei and cloud droplet measurements during ACE-2, *Tellus B*, 52, 828–842, 2000.
- Snider, J. R., Guibert, S., Brenguier, J.-L., and Putard, J.-P.: Aerosol activation in marine stratocumulus clouds: 2. Köhler and parcel theory closure studies, *J. Geophys. Res.*, 108, 8629, doi:10.1029/2002JD002692, 2003.
- 10 Stevens, B. and Feingold, G.: Untangling aerosol effects on clouds and precipitation in a buffered system, *Nature*, 461, 607–613, 2009.
- Springston, S. R., Kleinman, L. I., Nunnermacker, L. J., Brechtel, F., Lee, Y.-N., and Wang, J.: Chemical evolution of an isolated power plant plume during the TexAQs 2000 study, *Atmos. Environ.*, 39, 3431–3443, 2005.
- 15 Twohy, C. H., Petters, M. D., Snider, J. R., Stevens, B., Tahnk, W., Wetzal, M., Russell, L., and Burnet, F.: Evaluation of the aerosol indirect effect in marine stratocumulus clouds: droplet number, size, liquid water path, and radiative impact, *J. Geophys. Res.*, 110, D08203, doi:10.1029/2004JD005116, 2005.
- 20 Wang, J., Daum, P. H., Yum, S. S., Liu, Y., Senum, G. I., Lu, M.-L., Seinfeld, J. H., and Jonsson, H.: Observations of marine stratocumulus microphysics and implications for processes controlling droplet spectra: Results from the Marine Stratocumulus/Stratocumulus Experiment, *J. Geophys. Res.*, 114, D18210, doi:10.1029/2008JD011035, 2009.
- Weber, R. J., Clarke, A. D., Litchy, M., Li, J., Kok, G., Schillawski, R. D., and McMurry, P. H.: Spurious aerosol measurements when sampling from aircraft in the vicinity of clouds, *J. Geophys. Res.*, 103, 28337–28346, 1998.
- 25 Wood, R., Bretherton, C., Huebert, B., Mechoso, C. R., and Weller, R.: VOCALS-SouthEast Pacific Regional Experiment (REx) Scientific Program Overview, available at: http://www.eol.ucar.edu/projects/vocals/documentation/vocals_overview.pdf (last access: January 2011), June 2007.
- 30 Wood, R., Mechoso, C. R., Bretherton, C. S., Weller, R. A., Huebert, B., Straneo, F., Albrecht, B. A., Coe, H., Allen, G., Vaughan, G., Daum, P., Fairall, C., Chand, D., Gallardo Klenner, L., Garreaud, R., Grados, C., Covert, D. S., Bates, T. S., Krejci, R., Russell, L. M., de Szoeke, S., Brewer, A., Yuter, S. E., Springston, S. R., Chaigneau, A., Toniazzi, T., Min-

17318

nis, P., Palikonda, R., Abel, S. J., Brown, W. O. J., Williams, S., Fochesatto, J., Brioude, J., and Bower, K. N.: The VAMOS Ocean-Cloud-Atmosphere-Land Study Regional Experiment (VOCALS-REx): goals, platforms, and field operations, *Atmos. Chem. Phys.*, 11, 627–654, doi:10.5194/acp-11-627-2011, 2011.

17319

Table 1. Aerosol and cloud droplet instruments.

Instrument	Primary function	D_p range
CPC3025 ¹	Total aerosol	> 3 nm
CPC3010 ¹	Total aerosol	> 10 nm
SMPS (DMA) ²	Aerosol mobility size spectra	15–440 nm
PCASP ³	Cabin	0.11–3 μ m
PCASP ³	Pylon	0.11–3 μ m
CAS	Cloud droplet	0.6–56 μ m
CIP	Drizzle	8–940 μ m
AMS	Aerosol composition	60–600 nm
PILS	Aerosol composition	< 2 μ m

¹ DMT.

² TSI Inc., model 3081 DMA and model 3010 condensation particle counter.

³ PCASP-100X (Particle Measuring Systems, Inc., Boulder, CO) with SPP-200 electronics (Droplet measurement Technologies, Boulder, CO).

17320

Table 2. Cloud sampling intercomparisons.

Platform	Date	G-1			Other aircraft		
		CD	LWC	Time ¹	CD	LWC	Time ¹
TO	26 Oct	402	0.16	10:47–10:52	335	0.14	10:54–11:04
C130	4 Nov	226	0.10	11:28–11:35	203	0.16	11:25–11:33
BAe-146	12 Nov	47.3 ²	0.0065 ²	12:49–12:56	29.3	0.0095	12:45–15:51

¹ Rounded off to nearest minute.

² Maximum values $\sim 400 \text{ cm}^{-3}$, 0.1 g m^{-3} , in-cloud for ~ 1 min.

17321

Table 3. Definition of atmospheric layers.

Variable ¹	Marine boundary layer	Data subset		
		Pre-cloud	In-cloud	Above-cloud
Altitude (m)	< 800	Below and within 15 km of cloud	> 600	> 1200
RH (%)	n/a	< 90	n/a	n/a
Theta (°C)	n/a	n/a	n/a	> 22
LWC (g m^{-3})	< 0.01	< 0.01	> 0.02 LWC _{avg} > 0.05	< 0.01

¹ Condition applies to each 1 s time period within averaging time, except for LWC_{avg} which is an average value over a 1 min SMPS scan.

17322

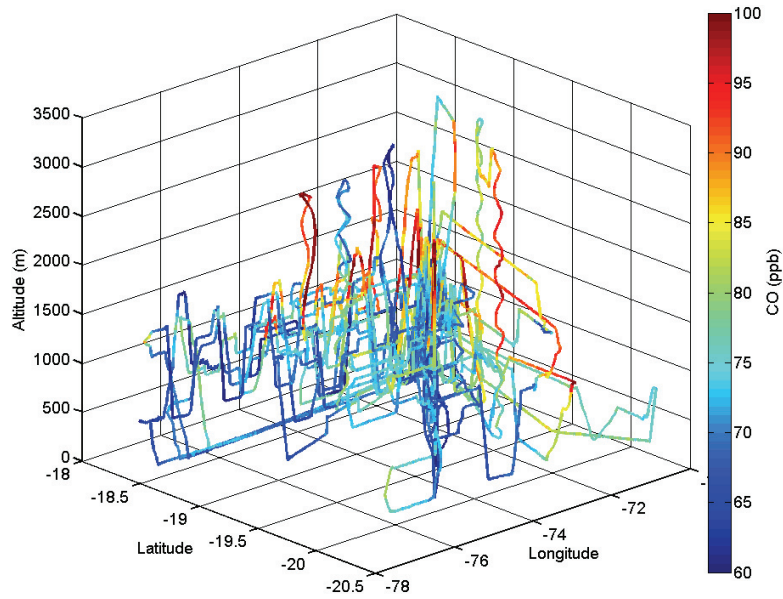


Fig. 1. Ground track of G-1 color coded by CO concentration. A portion of one flight south of -20.5 latitude not shown.

17323

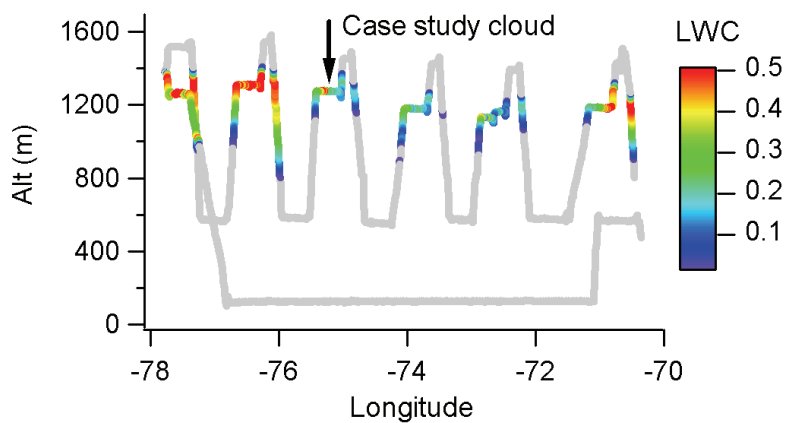


Fig. 2. Longitude–altitude cross section of flight track for 081028a color coded for cloud liquid water content in g m^{-3} . Cloud at -75.2° W longitude is used to illustrate anti-correlation between cloud droplets and interstitial aerosol.

17324

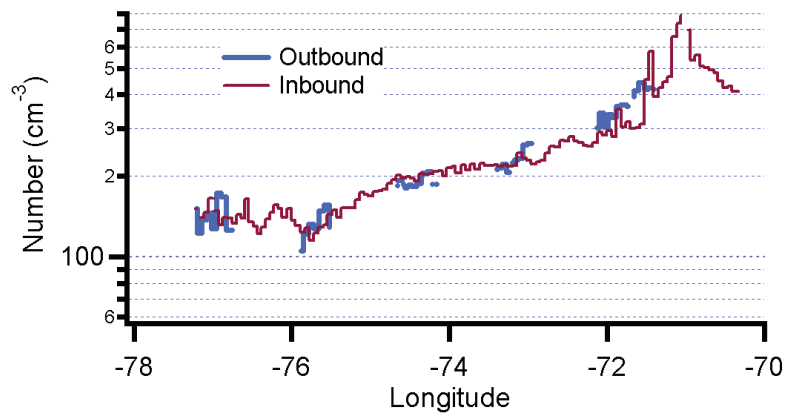


Fig. 3. Below cloud level SMPS measurement of number of particles with $D_p > 75$ nm.

17325

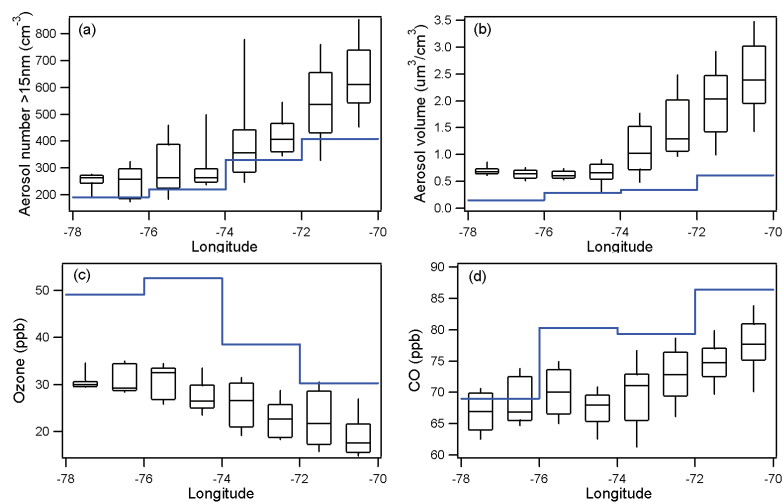


Fig. 4. Box plot showing frequency distribution of below cloud measurements of (a) aerosol number concentration and (b) volume measured by SMPS, (c) O₃, and (d) CO. Box indicates the 25th to 75th percentile range with line for median. Whiskers show 10th and 90th percentile values. Blue lines indicate the median values of FT observation divided into two degree longitude bins.

17326

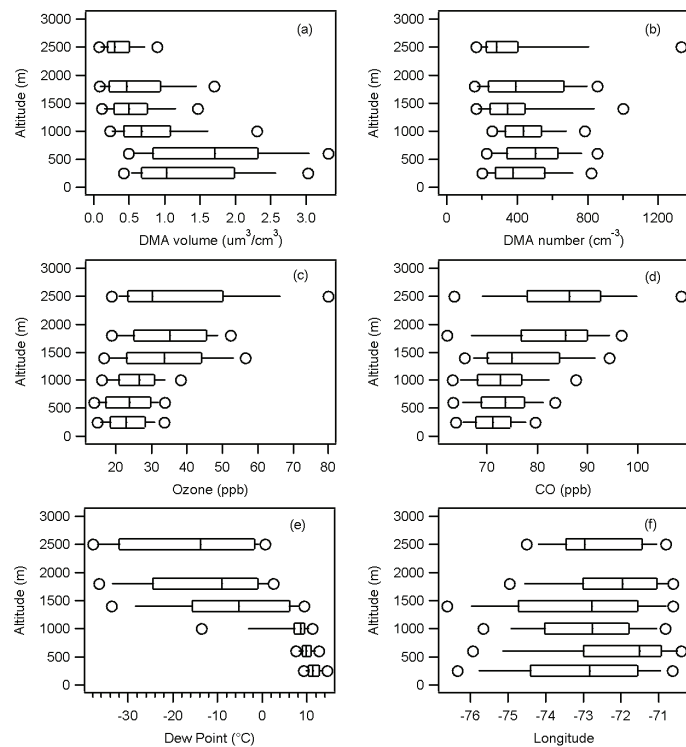


Fig. 5. Frequency distribution as a function of altitude. Box indicates the 25th to 75th percentile range with line for median. Whiskers show 10th and 90th percentile values. Circles are 5th and 95th percentile. Altitude bins are 100–400 m, 400–800 m, 800–1200 m, 1200–1600 m, 1600–2000 m, and above 2000 m.

17327

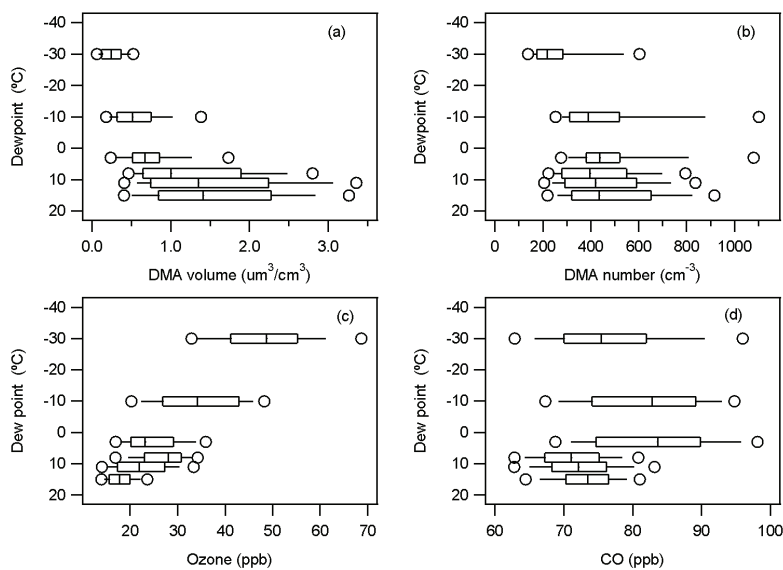


Fig. 6. Frequency distribution as a function of dew point. Box plot format same as in Fig. 5. Dew point bins are 16 to 12 °C, 12 to 10 °C, 10 to 6 °C, 6 to 0 °C, 0 to -20 °C, -20 to -40 °C. Qualitatively, the first 2 bins are below cloud, the third bin in the cloud layer, and the driest 3 bins above cloud.

17328

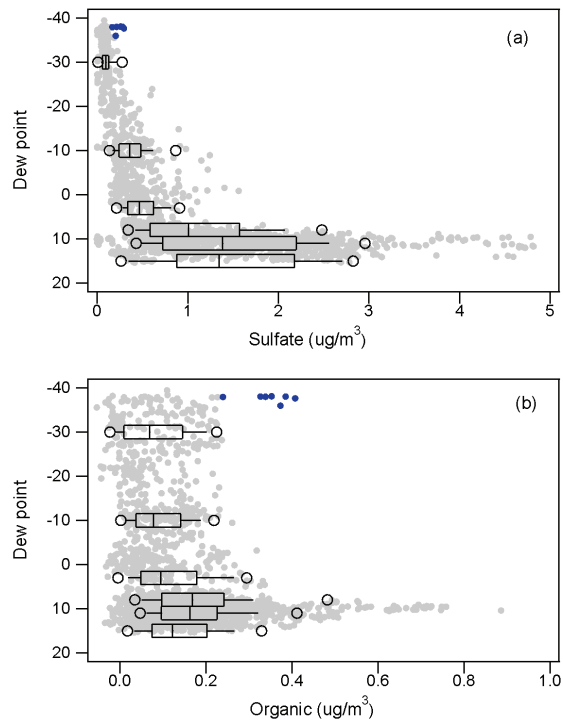


Fig. 7. Box plot showing frequency distributions for **(a)** sulfate and **(b)** organic aerosol measured with the AMS as a function of dew point. Box plot has same format as in Fig. 5. Each gray point represents data averaged over a DMA scan. Data points with $LWC > 0.01 \text{ g m}^{-3}$ are excluded. Blue points are 7 min of measurements in an organic rich plume on 25 October.

17329

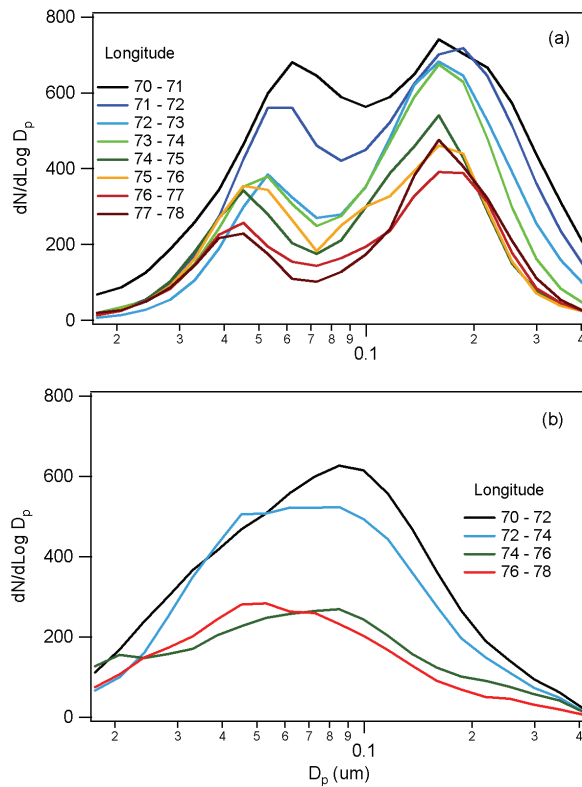


Fig. 8. Aerosol size distribution measured with SMPS **(a)** below cloud layer and **(b)** above cloud layer.

17330

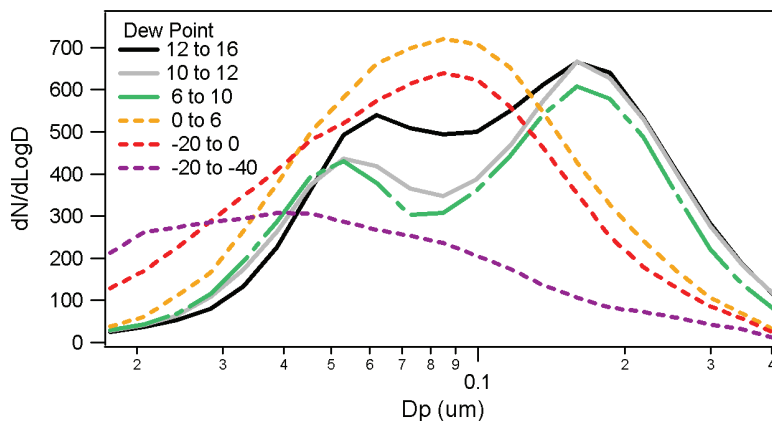


Fig. 9. Aerosol size distribution in cloud-free air from the SMPS as a function of dew point. Qualitatively, dew points from 10 to 16°C are located below cloud, 6–10°C is the cloud layer, and dew points below 6°C are in the free troposphere, above cloud.

17331

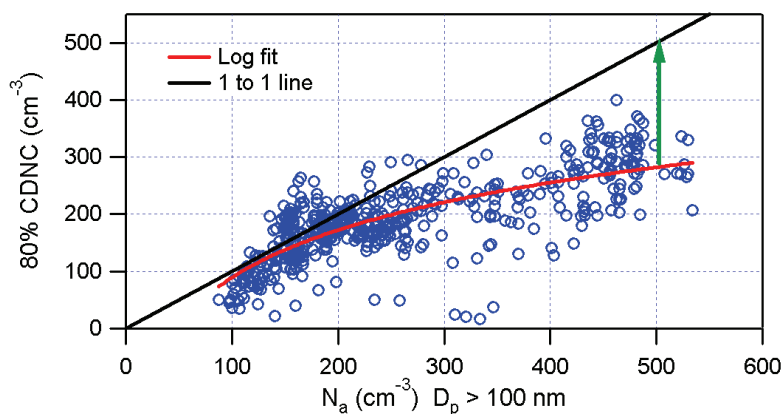


Fig. 10. Cloud droplet number concentration (CDNC) as a function of pre-cloud aerosol with $D_p > 100$ nm. Each data point is ~ 1 min of in-cloud data and an average of several minutes of aerosol data identified as pre-cloud. Broken clouds are eliminated. CDNC has been multiplied by 0.8. Equation of red line, after multiplying CDNC by 0.8, is $CDNC = -463 + 276 \log_{10}(N_a)$. Data points above line are due to activation of aerosol smaller than 75 nm or imprecision in indentifying pre-cloud air. Green arrow illustrates number of interstitial aerosol with $D_p > 100$ nm that give number balance between below and in-cloud particles, placed at $N_a = 500 \text{ cm}^{-3}$ for illustration.

17332

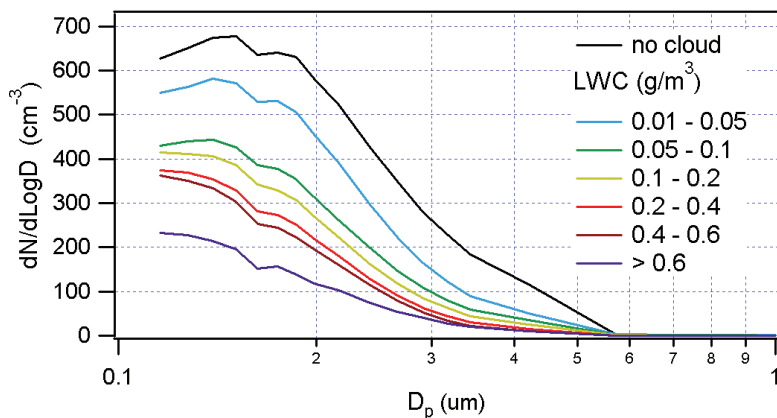


Fig. 11. Interstitial aerosol measured with in-cabin PCASP as a function of LWC. Reference “no-cloud” spectra is an average over all 1 s intervals on 102 cloud transects in which LWC < 0.01 g m⁻³. PCASP size range extends to 3 μm but is indistinguishable from zero on a linear scale. The discontinuity at 160 nm is located at the intersection of two instrument ranges.

17333

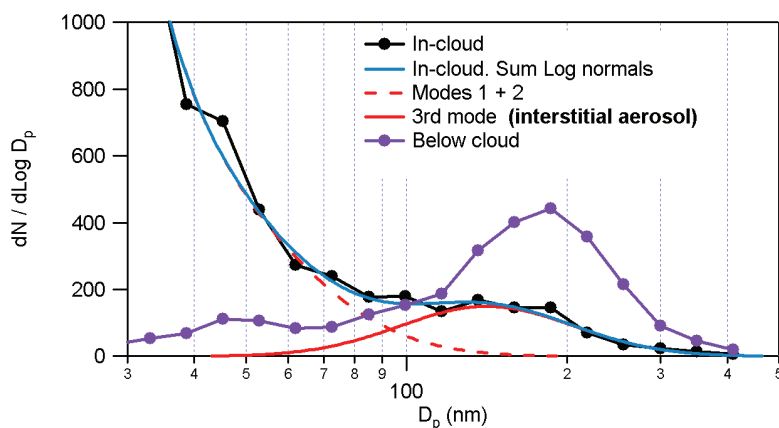


Fig. 12. In and below-cloud SMPS size distributions from the 28 October case study cloud. Black circles are in-cloud SMPS measurements which have been fit to a sum of 3 log normals (blue line). The 3rd mode is identified as interstitial aerosol. The dashed red line indicates the sum of the 2 smaller modes which in this case make a minor contribution to number concentration in the PCASP size range. For comparison the purple trace is below-cloud aerosol. Points in both SMPS size distributions are joined by straight lines for easy visualization.

17334

